Dalton Transactions

ROYAL SOCIETY OF CHEMISTRY

PAPER

View Article Online
View Journal | View Issue

Cite this: *Dalton Trans.*, 2025, **54**, 13540

Collapse or capture? Guest-induced response of two structurally distinct pillared-MOFs upon exposure to pyridines and quinolines

Dario Giovanardi, [a] Giorgio Cagossi, [a] Pavel N. Zolotarev,[b] Paolo P. Mazzeo, [a] Alessia Bacchi, [a] Lucia Carlucci, [b] Davide M. Proserpio [b] and Paolo Pelagatti *[a,c]

The response of two differently entangled, Zn-containing, pillared metal–organic frameworks (MOFs) toward quinolines and pyridines was studied. The corresponding products have been defined by single crystal X-ray diffraction analysis, when possible through single-crystal-to-single-crystal transformations. These two MOFs have similar chemical compositions, each consisting of a dicarboxylate linker (4,4′-biphenyldicarboxylate or 2,6-naphthalenedicarboxylate) and the same bis-amide-bis-pyridine pillar. The flexible and interpenetrated MOF **PUM168** and the rigid and polycatenated **PUM210** exhibit good uptake propensity towards quinoline, although structural modelling of all the included guest molecules was successful only for **PUM168**. For **PUM210**, only one molecule of quinoline coordinated to a metal center was modeled, whereas the remaining molecules were randomly distributed along the channels. The **PUM168** and **PUM210** crystals rapidly degraded once in contact with liquid pyridines. The decomposition products of **PUM210** in pyridine were structurally characterized, giving insights into the degradation pathway. This involves the replacement of the bis-amide-bis-pyridine pillar by pyridine with the formation of a new homoleptic 1D-coordination polymer in which Zn ions are bound to naphthalenedicarboxylate dianions and pyridine molecules. Finally, the uptake of the chelating 8-hydroxyquinoline by **PUM168** led to the protonolysis of the dicarboxylate linker and the extraction of Zn ions from the framework, with formation of the bis-chelate complex Zn(8-hydroxyquinolinate)$_2$.

Received 5th June 2025,
Accepted 12th August 2025

DOI: 10.1039/d5dt01321f

rsc.li/dalton

Introduction

Since their emergence, the use of metal organic frameworks for the inclusion of organic molecules has been a topic of interest.[1,2] Introducing active guest molecules in structurally well-defined materials is of paramount importance for understanding how host–guest interactions are responsible for their uptake. The advantage of using MOFs is related to their high crystallinity, which makes it feasible to precisely describe the supramolecular organization adopted by the included guest molecules. This approach is based on the so-called crystallization sponge method,[3] where crystalline containers, such as ad-hoc tailored MOFs, are used for the ordered inclusion of guest molecules.[4,5] The final result is a crystal that can be analysed by single-crystal X-ray diffraction, allowing the structural characterization of the included guest. This set-up opens up the possibility to structurally elucidating molecules, even when these are liquids or solids reluctant to crystallization. This topic has been recently reviewed.[6] A precise knowledge of the host–guest interactions in the loaded crystal is also fundamental for understanding and tuning how the guest is released from the crystal, which is of relevance for the controlled delivery of active guest compounds.

Over the last years, we have described the host capacity of the mixed-ligand MOF **PUM168** (PUM: "Parma University Materials") towards a series of oxygen-containing guests.[7–9]

PUM168 is formed by Zn-paddle-wheels containing 4,4′-biphenyldicarboxylate dianions, pillared by di-isonicotinoyl linkers, hereinafter named **L1**, containing the same biphenyl scaffold (Fig. 1, left). The triple interpenetrated framework gives rise to meandered microporous channels whose sizes are compatible with the inclusion of a pool of small organic molecules. In pristine crystals, the channels are filled with molecules of DMF, some of which are hydrogen bonded to the amide groups of the framework.

The massive uptake of naturally occurring liquid phenolic derivatives, such as the essential oil components eugenol,

[a]*Department of Chemical Science, Life Science and Environmental Sustainability, University of Parma, Parco Area delle Scienze 17/A, 43124 Parma, Italy. E-mail: paolo.pelagatti@unipr.it*
[b]*Dipartimento di Chimica, Università degli studi di Milano, 20133 Milano, Italy*
[c]*Interuniversity Consortium of Chemical Reactivity and Catalysis (CIRCC), Via Ulpiani 27, 70126 Bari, Italy*

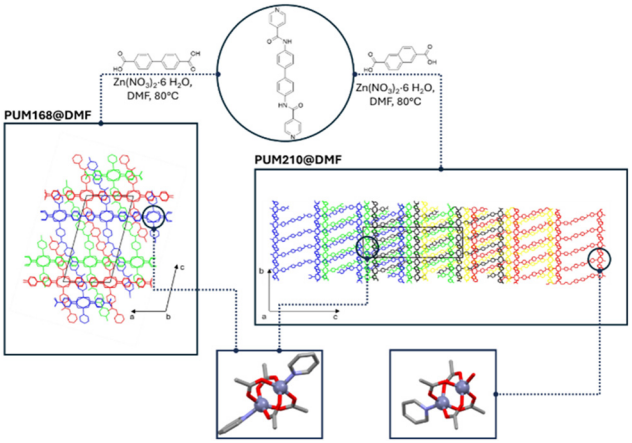

Fig. 1 Representation of the synthetic paths to obtain **PUM168** (left) and **PUM210** (right), along with the different entanglements and SBUs featuring the two MOFs.

thymol and carvacrol, was observed after native crystals were soaked in pure liquids or mixtures of these compounds. This process led to highly crystalline materials whose single-crystal X-ray diffraction analysis revealed the structural organization adopted by the included guest molecules and the structural rearrangements that the host framework underwent.[7,9] In detail, two different guest anchoring sites were recognized: the amide groups of the isonicotinoyl moiety and the carboxylate-containing paddle-wheels. In both cases, hydrogen bond interactions were responsible for guest stabilization. The distribution of the guest molecules between the two different receptor sites was guest-dependent and mainly governed by the steric requirements of the different included species.[9] In all cases, guest uptake triggered a structural rearrangement of the crystalline framework and involved a sliding of the MOF frames, preserving crystallinity. Within this frame of research activity, we became interested in studying the host-capacity of **PUM168** towards N-containing heterocycles, such as pyridines (PY) and quinolines (QUI). Although PY and QUI cannot be considered active compounds *per se*, they are used in several industrial and pharmaceutical processes, and their persistence, toxicity and potential impact on ecosystems pose serious concerns for their use.[10–12] For these reasons, their monitoring and removal from the environment by adsorbents is desired and their inclusion in coordination polymers is documented.[13–15] However, their coordinating capability makes them potentially reactive toward the metal centre contained in the SBU, which can translate into framework degradation. In fact, examples where the inclusion of molecules containing pyridine rings has been structurally elucidated are limited,[13,16–18] and in most of these limited cases, structural elucidation was derived from computational approaches.[19,20] The same remains true for quinolines.[14,21] Based on these premises, we became interested in studying the effect of N-heterocyclic guests on the structure of two pillared MOFs with distinct entanglement modes, focusing either on framework flexibility or guest uptake behaviour. In addition to **PUM168**, **PUM210**[22] was considered particularly well suited to study the effect of the presence of metal nuclei easily accessible by N-heterocyclic guests. Like **PUM168**, **PUM210** combines the coordination of **L1** and a dicarboxylate linker, 2,6-naphthalenedicarboxylate, to Zn(II), but displays parallel polycatenation (Fig. 1, right)[23] based on two different paddle-wheel SBUs, as reported in Fig. 1. One is a complete paddle-wheel of formula $[Zn_2(COO)_4(py)_2]$, while the other is a truncated paddle-wheel of formula $[Zn_2(COO)_4(py)(H_2O)]$, where a molecule of water takes the place of a pyridine-linker. The presence of a labile coordinated solvent is expected to facilitate the binding of the guest molecule, as we observed when using a porous MOF containing Cu-paddle-wheels after a pre-coordinated water molecule was removed.[16] Moreover, compared to **PUM168**, the polycatenated framework of **PUM210** is less dynamic, as observed during repeated manipulations, like transmetallation,[22] thermal activation[24] and the inclusion of phenol derivatives.[25] The coordinative unsaturation of the SBU is then expected to promote guest binding, while flexibility is expected to promote guest inclusion.

We selected, as reported in Chart 1, a collection of N-containing heterocycles, which although different from phenols, can only function as hydrogen bond acceptors through the heteroatom, except when functionalized with proper hydrogen-bond specific groups, like in the case for 3-hydroxymethylpyridine, 4-aminomethylpyridine and 8-hydoxyquinoline. The interactions of the type $N_{py}\cdots H–N(C{=}O)$ with the amide groups installed in the MOF framework can then be envisaged. Hence, in this study, we describe how the crystals of **PUM168** and **PUM210** respond to a series of liquid, N-containing, heterocycle guests (Chart 1).

When possible, the pristine crystals (**PUM168@DMF** and **PUM210@DMF**) were soaked in a neat liquid of the guest, following the same protocols developed for the uptake of essen-

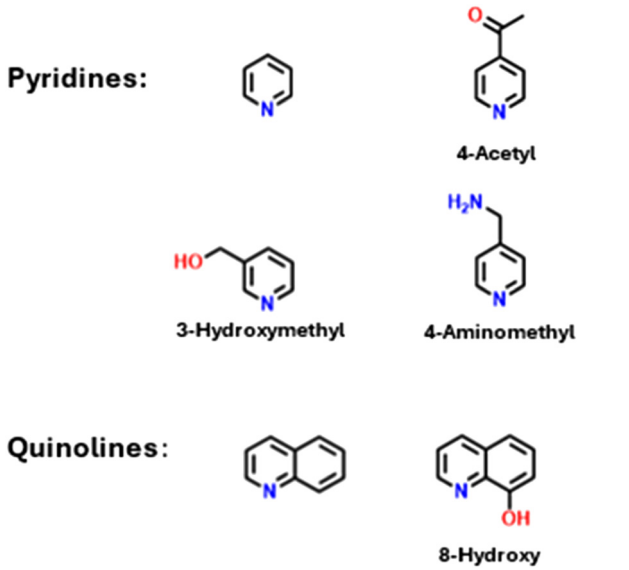

Chart 1 Structural schemes of the N-heterocyclic guests used in this study.

tial oil components.[7,9] When necessary, like in the case of 8-OH-QUI, acetonitrile solutions of the guest were used. In these cases, the crystals of **PUM168@DMF** were first converted into **PUM168@ACN**[26] prior to soaking. The guest-exchange processes were monitored by ^{1}HNMR, TGA and, whenever applicable, by single-crystal X-ray diffraction analysis. Particular attention was given to the stability of the MOF crystals towards the different guests, highlighting the guest-induced structural transformations.

Experimental

Materials and methods

PUM168 and **PUM210** were prepared according to the reported procedure.[7,22] Pyridines (PY: pyridine, 4-acetyl pyridine, 3-hydroxymethyl pyridine and 4-aminomethyl pyridine) and quinolines (QUI: quinoline and 8-hydorxy-quinoline) were commercially available and used as received.

Soaking experiments

The soaking experiments were conducted using crystals of **PUM168@DMF**, **PUM210@DMF** and **PUM168@ACN**. The ACN solvated crystals were used when necessary to dissolve the solid guest in the same solvent. Acetonitrile was selected since it does not damage the MOF crystals and it is able to completely remove the DMF contained in the pristine crystals without significantly affecting the potential void of the same. The DMF-ACN exchange was conducted as previously reported,[26] at room temperature for the desired time and the crystals were visually inspected for possible crystal deterioration. A part of the crystals was then collected and analyzed by ^{1}HNMR, TGA and, when possible, by SC-XRD analysis.

General procedure for the preparation of the samples

The TGA and ^{1}H NMR analyses were conducted after gently drying the crystals over a filter paper to remove the solvent molecules covering the crystal surface. When crystal fragmentation was evident, the presence of an exclusive crystalline phase was ascertained by using X-ray data on the crystals of different sizes.

Thermogravimetric analyses

Thermogravimetric analyses (TGA) were performed with a PerkinElmer TGA 8000 instrument (mass of sample: 2–5 mg) in a Pt crucible under a non-reductive atmosphere (air flux 30 mL min^{-1}) in the temperature range of 30–500 °C at 10 °C min^{-1}. Higher temperatures were not applied to avoid possibly damaging the crucible due to the high metal content of the samples.

FT-IR spectroscopy

FT-IR spectra were recorded in the range of 400–4000 cm^{-1} using a PerkinElmer Spectrum Two FT-IR spectrophotometer coupled with a PerkinElmer UATR accessory and a diamond crystal plate.

^{1}H NMR Spectroscopy

^{1}H NMR spectra were recorded on a Bruker Avance spectrometer operating for ^{1}H at 400 MHz at 25 °C after dissolving the sample in CF_3COOD (TFA-d) and diluting it with $(CD_3)_2SO$ (DMSO-d_6). Chemical shifts (δ) are expressed in ppm relative to the residual peak of deuterated DMSO (^{1}H = 2.50 ppm).

Single-crystal X-ray diffraction

Single-crystal X-ray diffraction analyses of **PUM168@(quino)$_1$**, **PUM168@(quino)$_7$** were performed on a Bruker D8 Venture diffractometer equipped with a kappa goniometer, an Oxford Cryostream, and a Photon II detector using microfocused Cu Kα radiation (λ = 1.54178 Å). Crystals of **PUM210@(quino)$_1$** and **PUM210_PY** were mounted over a Bruker D8 Venture diffractometer equipped with a kappa goniometer, an Oxford Cryostream and a Photon III detector, using microfocused Mo Kα radiation (λ = 0.7107 Å). Prior to X-ray diffraction analysis, the crystals were dipped in a drop of Fomblin oil to avoid the loss of the guest. Lorentz polarization and absorption corrections were applied for all the experiments. Data reduction was carried out using APEX v5 software. The structures were all solved by direct methods using SHELXT[27] and refined by full-matrix least squares on all F^2 using SHELXL,[28] as implemented in Olex2.[29] Anisotropic thermal displacement parameters were used for all non-hydrogen atoms. Calculations of the unmodelled solvent electron densities were carried out by applying cycles of SQUEEZE/PLATON[30] on the structures, namely **PUM210@(quino)$_1$**, **PUM168@(quino)$_7$** and **PUM168@(quino)$_1$**. Table 1 reports the parameters and refinement results for the collected crystallographic data. The crystallographic data of **PUM168@(quino)$_1$**, **PUM168@(quino)$_7$**, **PUM210@(quino)$_1$** and **PUM210_PY** have been deposited in the CSD with CCDC code 2450670, 2450672, 2450671 and 2450669, respectively. The use of @ in the names of the materials indicates guest inclusion, while the use of an underscore (_) refers to the decomposition product derived from contact with the guest.

Results and discussion

Soaking experiments with PUM168

The three-fold interpenetrated framework of **PUM168@DMF** contains meandered channels that represent about 50% of the total cell volume (Mercury, probe radius of 1.2 Å).[7] The aperture of the channels is 7.1 × 15.1 Å^2, which is compatible with the inclusion of small organic molecules. In the pristine material, 12 DMF molecules fill the voids of the framework, with some of them being hydrogen bonded to the amide groups of the pillar. Several O-containing guests have already been hosted in **PUM168** through soaking experiments, where the initially-included DMF was replaced by the incoming guest.[7,9,26] To favor the occurrence of host–guest contacts, and make good uptake more feasible, in addition to pure pyridine, three liquid PY species containing hydrogen-bonded active substituents, such as carbonyl (4-acetylpyridine), hydroxyl

Table 1 Crystallographic tables for the four structures reported: **PUM168@(quino)$_7$**, **PUM168@(quino)$_1$**, **PUM210@(quino)$_1$** and **PUM210_PY**

Identification code	**PUM168@(quino)$_7$**	**PUM168@(quino)$_1$**	**PUM210@(quino)$_1$**	**PUM210_PY**
Empirical formula	$(C_{78}H_{51}O_{15}N_6Zn_3)(C_3H_7NO)(C_9H_7N)_{6.75}$	$(C_{78}H_{51}O_{15}N_6Zn_3)(C_2H_3N)_{8.5}(C_9H_7N)_{0.75}$	$(C_{84}H_{51}O_{19}N_6Zn_4)(C_9H_7N)_2(C_3H_7NO)$	$C_{37}H_{31}N_5O_4Zn$
Formula weight	2453.25	1954.18	1985.13	675.04
Temperature/K	200.00	200.00	150.00	200
Crystal system	triclinic	triclinic	triclinic	Monoclinic
Space group	$P\bar{1}$	$P\bar{1}$	$P\bar{1}$	$P2/n$
a/Å	15.2374(3)	15.0514(7)	13.1342(9)	9.7431(13)
b/Å	15.2428(3)	15.0686(8)	13.1346(8)	9.2259(10)
c/Å	27.0220(5)	26.8387(12)	31.665(2)	17.642(2)
α/°	96.3530(10)	86.567(3)	87.768(2)	90
β/°	98.1620(10)	78.620(3)	87.468(2)	98.650(13)
γ/°	90.3930(10)	60.082(3)	86.876(2)	90
Volume/Å^{-3}	6172.8(2)	5166.9(5)	5445.6(6)	1567.7(3)
Z	2	2	2	2
$\rho_{calc,}$ g cm^{-3}	1.320	1.256	1.211	1.430
μ/mm^{-1}	1.261	1.365	0.936	0.833
F(000)	2540.0	2018.0	2034.0	700.0
Crystal size/mm^{-3}	0.025 × 0.022 × 0.018	0.021 × 0.018 × 0.015	0.025 × 0.02 × 0.015	0.025 × 0.02 × 0.018
Radiation	CuKα (λ = 1.54178)	CuKα (λ = 1.54178)	MoKα (λ = 0.71073)	Mo Kα (λ = 0.71073)
2θ range for data collection/°	5.836 to 140.132	6.726 to 141.204	3.866 to 50.054	7.3 to 51.354
Index ranges	$-18 \le h \le 18$, $-18 \le k \le 18$, $-32 \le l \le 32$	$-18 \le h \le 18$, $-18 \le k \le 18$, $-32 \le l \le 31$	$-15 \le h \le 15$, $-12 \le k \le 15$, $-36 \le l \le 37$	$-11 \le h \le 11$, $-11 \le k \le 11$, $-21 \le l \le 21$
Reflections collected	146 003	100 135	110 594	11 881
Independent reflections	23 360 [R_{int} = 0.0587, R_{sigma} = 0.0337]	19 665 [R_{int} = 0.0917, R_{sigma} = 0.0615]	19 068 [R_{int} = 0.1175, R_{sigma} = 0.1028]	2983 [R_{int} = 0.0756, R_{sigma} = 0.0784]
Data/restraints/parameters	23 360/1134/1696	19 665/612/1192	19 068/298/1041	2983/0/221
Goodness-of-fit on F^2	1.041	1.043	1.060	1.017
Final R indexes [$I \ge 2\sigma(I)$]	R_1 = 0.0789, wR_2 = 0.2335	R_1 = 0.1098, wR_2 = 0.3243	R_1 = 0.0984, wR_2 = 0.2507	R_1 = 0.0468, wR_2 = 0.0798
Final R indexes [all data]	R_1 = 0.0933, wR_2 = 0.2503	R_1 = 0.1457, wR_2 = 0.3616	R_1 = 0.1361, wR_2 = 0.2760	R_1 = 0.0806, wR_2 = 0.0885
Largest diff. peak/hole/e Å^{-3}	0.96/−0.94	1.58/−0.98	2.05/−1.15	0.32/−0.30

(3-hydroxymethylpyridine) or amino (4-aminomethylpyridine) groups (Chart 1) were selected. The molecular volume of the guests (pyridine = 87 Å^3, 3-hydroxymethylpyridine = 111 Å^3, 4-aminomethylpyridine = 115 Å^3, 4-acetylpyridine = 125 Å^3, and quinoline = 135 Å^3)[31] are compatible with the pore dimensions of **PUM168**, corresponding to a calculated potential void of 3059 Å^3. With these species, interactions involving the pyridine nitrogen or the hydrogen-bond active functionality with the amide groups of the framework can be envisaged. Since these compounds are liquids at room temperature, the pristine crystals of **PUM168@DMF** were soaked in the neat liquids, following the same procedure adopted with the essential oil components.[7,9] Optical microscopy evidenced the immediate opacification and bleaching of the crystals once in contact with the guest (see Fig. S1 and S2). The crystals turned out to be no longer suitable for single-crystal X-ray analysis. Within 24 hours, the crystals had severely fragmented into thin plates (see Fig. S2), which were again not suitable for structural characterization. SEM inspection revealed profound fractures of the crystals, likely responsible for the observed crystal fragmentation (see Fig. S19). Prolonging the soaking for several days led to the pulverization of the crystals. XRPD analysis indicated the formation of different phases with some peaks related to the ligand **L1**. Nonetheless, the ^{1}H NMR and TGA analyses conducted on the fragmented crystals indicated the presence of the guest (see Fig. S4–S6 for ^{1}HNMR, Fig. S12–S14 for TGA). Similar phenomena were reported in the literature for the formation of 2D nanosheets starting from 3D architectures.[32] Different behaviour was observed with pure quinoline. Although a partial reduction of the crystals' dimension was visible, soaking did not lead to excessive crystal degradation, as visualized by SEM inspection (see Fig. S20). Moreover, the crystals were suitable for structural characterization. Structural analysis evidenced that the MOF framework had practically retained its initial structure, as can be inferred from Fig. 1 and 2 (left). Even the relative orientation of the amide groups of the interpenetrated frames was the same found in the pristine **PUM168@DMF**. Two frames display the amide groups in an acentric cisoidal orientation, while the third frame contains the amide groups in a transoidal orientation. The quinoline molecules replaced most of the pristine molecules of DMF, except for one DMF molecule that was hydrogen bonded to an amide group of the centric transoidal net. Structural analysis led to the modelling of the 6 molecules of quinoline that were sorted around the asymmetric unit as depicted in Fig. 2 (right, named Q1–Q6). All had full occupancy except for Q3, which displayed a 0.5 occupancy. Among the included guests, only Q3 and Q4 were hydrogen bonded to the amide functions of

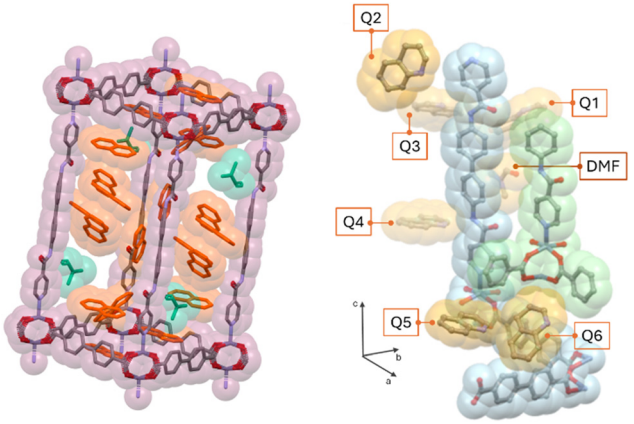

Fig. 2 Left: A single cage of **PUM168@(quino)$_7$** showing the efficient packing of the quinolines in the pores. For clarity, only one of the three interpenetrated frames is reported. Color code: quinoline orange, DMF green. Right: Distribution of the modelled quinoline molecules in **PUM168@(quino)$_7$** around the asymmetric unit of **PUM168**. The modelling of the seventh molecule of quinoline was not possible.

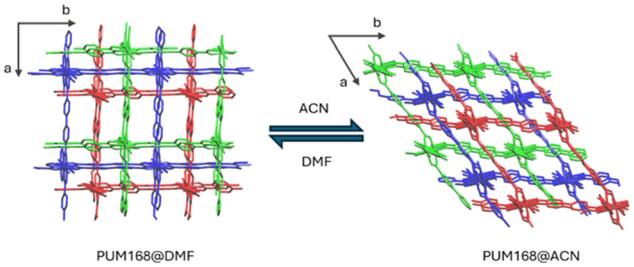

Fig. 3 Representation of the two frameworks of **PUM168@DMF** (pristine) and **PUM168@ACN** (after DMF-to-ACN exchange).

the acentric net. The efficient packing of the quinoline molecules inside the cavities of the framework left only a calculated residual electron density of 85 electrons. The ^{1}H NMR spectrum of the digested crystals was indicative of seven molecules of quinoline and one molecule of DMF per asymmetric unit (see Fig. S7). The 85 residual electrons can be attributed to 1.25 molecules of the disordered quinolines (see Fig. S27). These results indicate very good agreement between the number of quinoline molecules that were structurally determined (6.75), and the same number guests determined by NMR (7). As already observed with phenolic guests,[25] the TGA trace of **PUM168@(quino)$_7$** (Fig. S15) showed a step-wise profile, which is in agreement with the high flexibility expected for the framework. In the 30–300 °C temperature range, the weight loss accounted for about 39%, which is in perfect agreement with the observed amount of quinoline determined by ^{1}H NMR (36% related to the seven included molecules) and a residual molecule of DMF (with an expected value of 3%). For simplicity, this material will hereinafter be referred to as **PUM168@(quino)$_7$**.

In an attempt to mitigate the crystal degradation observed with the PYs, soaking experiments were repeated using 0.1 M acetonitrile solutions of the guest. Based on our previous findings, acetonitrile is well tolerated by crystals of the MOF, allowing for the complete removal of DMF,[26] and the formation of **PUM168@ACN**. Although it is known that solvent exchange leads to a structural deformation of the MOF framework, mainly involving the 2D square nets (Fig. 3 and Fig. S30 and S31),[26] the potential void of **PUM168@ACN** (2424 Å^3, 46.1% of the unit cell volume) is enough to ensure the accommodation of a rather large number of guest molecules. Nevertheless, once soaked, the crystals became opaque again, resulting in them becoming no longer suitable for X-ray structural characterization; hence, they were not characterized further. To evaluate the effect derived from the guest concentration, the crystals of **PUM168@ACN** were soaked in a 0.1 M acetonitrile solution of quinoline. The ^{1}HNMR revealed a much lower uptake, with the inclusion of only 0.75 molecules of quinoline per asymmetric unit after three days of soaking. This value did not change after soaking was prolonged for up to two weeks (see Fig. S8). Accordingly, TGA shows a weight loss of about 6.7% above 150 °C, in agreement with the calculated 6% relative to the presence of 0.75 molecules of quinoline.

The structural characterization confirmed the inclusion of one guest molecule, which displayed 0.75 chemical occupancy and was unexpectedly positioned in the distorted squares defined by the dicarboxylate linkers (Fig. 4). As for the previous inclusion product, for simplicity, this material will be referred to as **PUM168@(quino)$_1$**. The whole framework remained practically intact without significant variations with respect to that of the starting **PUM168@ACN**, indicating that the accommodation of the guest molecule did not have any evident structural effect (see Fig. S30 and S31).

The nitrogen atom of the included quinoline was not involved in any significant intermolecular contact; instead, its uptake was dictated by π–π stacking between quinoline and the biphenyl scaffold of the dicarboxylate linkers. The failed trap-

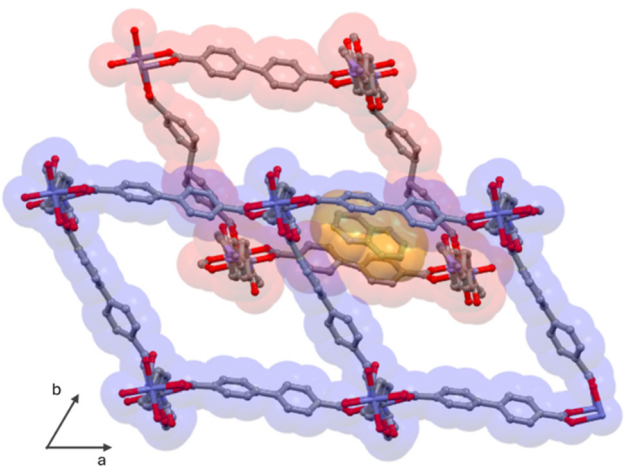

Fig. 4 Visualization of the quinoline molecule (colored in yellow) trapped in the distorted squares defined by the dicarboxylate linkers in the framework of **PUM168@(quino)$_1$**.

ping of the quinoline molecules along the framework channels is imputable to their rather high solubility in acetonitrile, which caused guest extraction from the crystal, as confirmed by the number of disordered ACN molecules distributed along the channels, as indicated by ^{1}HNMR analysis and the unmodelled residual electron density (see Fig. S28). Under these circumstances, quinoline was more conveniently arranged between the thin pocket offered by the polyaromatic carboxylate squares.

We then became interested in studying the effect of a chelating quinoline, such as 8-hydroxyquinoline (8-OH-quino).[33] This compound is solid at room temperature, and then, soaking was conducted in an acetonitrile solution (0.1 M) using crystals of **PUM168@ACN**. Once soaked, the crystals quickly became opaque (Fig. 5, top-left), and the solution turned light-yellow. After 24 hours, small yellow crystals started to appear on the surface of the MOF crystals, as depicted in Fig. 5 (top-right).

After three days, ^{1}H NMR and FTIR spectroscopy revealed that the yellow crystals were the bis-chelate complex, Zn(8-O-quino)$_2$[34–37] (see Fig. S10 and S11). This was further confirmed by a parallel reaction between 8-OH-quino and Zn(OAc)$_2$ in a 2 : 1 molar ratio, conducted in acetonitrile. The formation of the bis-chelate complex must have occurred through the protonolysis of one carboxylate linker, promoted by two equivalents of 8-OH-quino, with the formation of one equivalent each of 4,4′-diphenyldicarboxylic acid and the bis-chelate complex Zn(8-O-quino)$_2$, as depicted in Fig. 5 (bottom). This reaction led to the collapse of the MOF crystal framework. The subsequent crystallization of the quinoline complex on the surface of the MOF crystals can be explained by its poor solubility in acetonitrile. The degradation process appears to involve mainly the surface of the crystal, as evidenced by the observation that cutting a damaged crystal into two parts revealed still crystalline surfaces that turned opaque if brought into contact with the solution again (see Fig. S3).

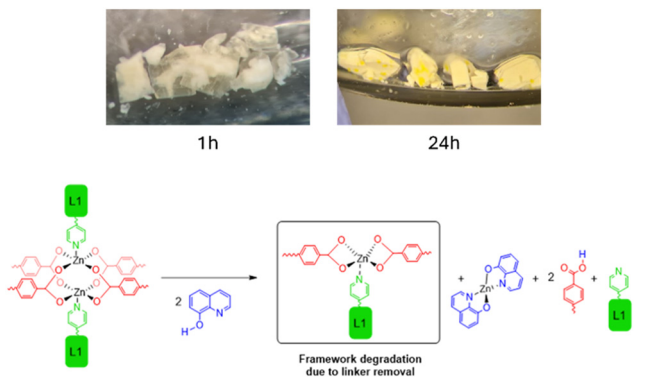

Fig. 5 Top-left: Opacification of the crystals of **PUM168@ACN** after soaking in a 0.1 M acetonitrile solution of 8-hydroxyquinoline. Top-right: appearance of the new crystalline phase corresponding to Zn(8-O-QUI)$_2$ on the surface of the damaged MOF crystals. Bottom: simplified reaction scheme.

Soaking experiments with PUM210

To gain insights into the effect derived from the type of entanglement and SBU in the framework on the guest-inclusion ability of the MOF, we moved our attention to the behavior of **PUM210@DMF** towards quinoline and pyridine. This MOF features polycatenated frames that contain two different SBU paddle-wheels and display a reduced dynamicity compared to **PUM168@DMF** (Fig. 1, right). The facile substitution of the water molecule contained in one of the SBUs was expected to promote the uptake of the N-heterocyclic guest by coordination with the metal. As already observed with **PUM168@DMF**, the crystals of **PUM210@DMF** also bleached when soaked in neat pyridine. After five days of soaking, white blocks and pale-yellow platelet crystals appeared (see Fig. S2, right). The EDX analysis of the selected crystals evidenced that only the white crystals contained Zn (see Fig. S21 and S22).

Single-crystal X-ray analysis revealed that the pale yellow crystals corresponded to **L1**,[38] while the white crystals were a new polymeric compound, hereinafter referred to as **PUM210_PY**, that were derived from the substitution of the bis-amide pillars by the pyridines, as depicted in Fig. 6. **PUM210_PY** crystallizes in the monoclinic space group *P*2/*n*. Each zinc atom has a trigonal bipyramidal coordination (Fig. 6a) satisfied by three pyridines and two bridging 2,6-naphthalene dicarboxylate anions to form 1D-coordination polymeric chains, as reported in Fig. 6b. The 1D chains are packed to form a 3D-network held together by dispersive forces between the coordinated pyridine rings (Fig. 6c). In the

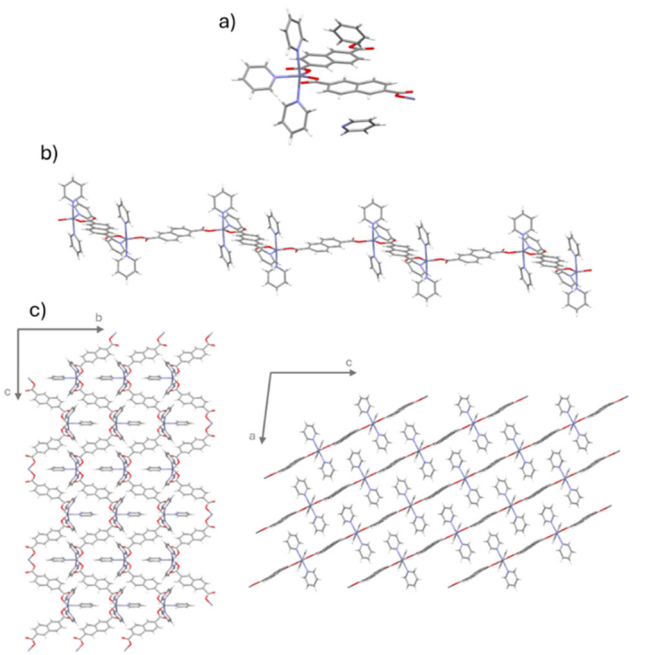

Fig. 6 (a) Asymmetric unit of **PUM210_PY** obtained by degradation of **PUM210@DMF** in pyridine. (b) Visualization of the mono-dimensional chain of the polymer and (c) visualization of the packing of the chains along the crystallographic axis *a* (left) and *b* (right), respectively. The included molecules of pyridine are not reported for clarity.

middle of the cavities, two molecules of the pyridines were modelled. Considering the result obtained with the pure pyridine, soaking with the substituted pyridines was not carried out. The crystals of **PUM210@DMF** showed a different behaviour towards neat quinoline. Once soaked, the crystals retained their crystallinity, although a certain degree of fragmentation and opacification was visible (see Fig. S21). However, the crystals were still suitable for single-crystal X-ray analysis. The structural characterization of the new material revealed a framework very similar to that of the starting **PUM210@DMF**, but now a molecule of quinoline was coordinated to the truncated SBU in place of water (Fig. 7 and 8, left).

This product can then be formulated as $[Zn_4(ndc)_4(\mathbf{L1})_{1.5}(QUI)]_n{\cdot}(DMF)_x$, hereinafter referred to as **PUM210@(quino)$_1$**. Compared to the pristine material, **PUM210@(quino)$_1$** retains the same four-fold polycatenation (Fig. 7). However, it presented a different relative disposition of the amides, with the central one retaining a transoidal arrangement, while the others adopted a cisoidal orientation (Fig. S32). In addition, the material retained its initial porosity (from 40% to 36% of calculated void of the unit cell volume). The disposition of the channel, however, changed. In the pristine material, the mono-dimensional channel runs along the crystallographic axis *b*, whereas in **PUM210@(quino)$_1$**, the same channel is located along the diagonal passing through the *a*,*b*-plane (see Fig. S33).

No molecule of quinoline could be modelled in the mono-dimensional channels, while two molecules of DMF were found interacting with an amidic moiety. The application of

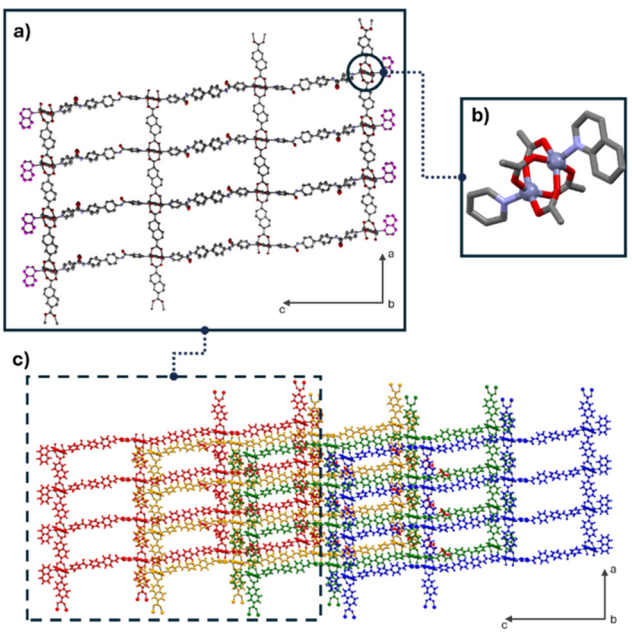

Fig. 7 (a) Visualization of a single frame of **PUM210@(quino)$_1$**, highlighting the coordinated quinoline in magenta. (b) View of the SBU of **PUM210@(quino)$_1$** showing the coordinated molecule of quinoline occupying the apical position of the Zn atom. (c) Polycatenation displayed by **PUM210@(quino)$_1$**, similar to that of the **PUM210@DMF**.[39]

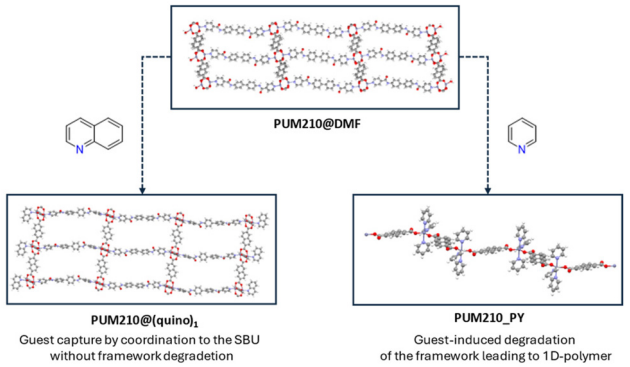

Fig. 8 Different reactivities shown by **PUM210@DMF** in neat quinoline (left) and pyridine (right). In **PUM210@(quino)$_1$** the modelled DMF molecules are not reported.

SQUEEZE/PLATON[30] cycles calculated only 48 electrons located in the channels running along the crystallographic axis *a* (see Fig. S29), consistent with an approximately 0.75 molecules of quinoline randomly distributed along the channels in a liquid-like configuration. The ^{1}H NMR spectrum of the digested crystals (see Fig. S9) was indicative of the presence of 2.5 molecules of DMF and about 12 molecules of quinoline per asymmetric unit, data which were further confirmed by TGA analysis (see Fig. S17). The thermal trace exhibits a two-step weight loss. The first step occurred below 150 °C and the weight loss did not exceed 40%, which is in agreement with the release of 11 molecules of quinoline. The second step occurred in the range of 150 °C–300 °C and corresponded to 13% weight loss, which is related to the release of another 2 molecules of quinoline and 2.5 molecules of DMF that were anchored to the framework.

Based on the results obtained with **PUM168@ACN**, soaking experiments involving 8-OH-QUI were not carried out.

Comparison of the different guest behaviours

The soaking experiments with quinolines and pyridines were conducted under identical conditions, using a large excess of the guest with respect to a few milligrams of crystals. Quinoline and pyridine are both good ligands for metal ions, as testified by the expansive literature concerning their coordination chemistry.[33,36,40] The potential porosity of both microporous frameworks appears sufficient to host several molecules of the two guests. However, the behavior shown by the two guests toward the MOF crystals is markedly different. Although quinoline is sterically more demanding than pyridine, it travelled along the MOF frameworks easily, as demonstrated by the massive inclusion observed with **PUM168@(quino)$_7$** (Fig. 2). Moreover, quinoline can also approach the paddle-wheel SBUs contained in the frameworks, as demonstrated by its coordination trapping found within **PUM210@(quino)$_1$** (Fig. 7, left). In no case did quinoline induce the displacement of **L1** and the crystals survived soaking. Comparatively, a totally different behavior was observed with the pyridines with both MOFs; it was revealed that they were

able to displace **L1** from the metal, as clearly demonstrated in the case of **PUM210_PY** (Fig. 7, right). This behavior can be rationalized by considering that pyridine is more basic than quinoline (pK_α values of 5.23 and 4.93, respectively)[41] and therefore more capable of competing for metal coordination with **L1**.[42] Noteworthy is the different mechanism of uptake shown by the two MOFs towards quinoline. In the flexible **PUM168**, which contains only complete paddle-wheel SBUs, quinoline molecules are hosted within the framework cavities, where they are stabilized by intermolecular contacts. In contrast, the rigid **PUM210** captures quinoline through coordination to the truncated paddle-wheel, while additional molecules are randomly distributed within the framework cavities.

Finally, protic and chelating quinolinic guests became disruptive for the MOF crystals, such as in the case of 8-OH-QUI. In this case, the framework collapsed owing to the protonolysis of the coordinating carboxylates and the removal of the Zn ions in the form of the bis-chelate complex Zn(8-O-QUI)$_2$.

Conclusions

In this work, we compared the hosting behaviour of N-heterocyclic guests in two microporous pillared MOFs that share similar chemical composition, but different entanglements. Significant guest inclusion was observed only in the case of pure quinoline, whereas the use of pyridines led to severe MOF degradation. For **PUM168@(quino)$_7$**, structural modelling of the included quinoline molecules was feasible and not limited to the molecules interacting with the amide functional groups of the framework. Conversely, in the case of **PUM210@(quino)$_1$**, modelling was possible only for a molecule of quinoline coordinated to the zinc atom, while the other molecules remained disorderly distributed along the channels of the framework. The different interactions offered by the two MOFs to the guest modelling are ascribable to their different flexibilities. The known adaptive behaviour of the flexible interpenetrated **PUM168@DMF** ensures that sufficiently robust host–guest interactions occur during the entry of the guest, allowing the guest to achieve stable positioning within the framework. This adaptive behaviour is not present in the case of the rigid polycatenated **PUM210@DMF**, limiting the guest modelling to the coordinated quinoline. This interpretation is supported by the TGA profiles of **PUM168@(quino)$_7$** and **PUM210(quino)$_1$**. However, all the tested MOFs were unstable towards pyridines, as evidenced by the fast degradation of their crystals. However, in the case of **PUM210@DMF**, its decomposition products were revealed by structural characterization. Here, the paddle-wheel SBUs were decomposed by the replacement of the pillar **L1** with pyridines, leading to the formation of the 1D-coordination polymer, **PUM210_PY**. The different tolerance shown by the two MOFs towards quinoline and pyridine cannot be associated with the different mobilities of the guest through the MOF framework but rather by their different coordination capabilities, where the more basic pyridine leads to a complete pillar replacement. Importantly, the use of a protic and chelating quinoline, such as 8-hydroxy-quinoline, leads again to fast SBU degradation, triggered by the protonolysis of the Zn–OOC bonds and the consequent removal of zinc from the MOF framework in the form of the bis-chelate complex Zn(8-O-QUI)$_2$. These findings are of paramount importance for all the researchers involved in the use of MOF crystals for their inclusion of or their interaction with biologically relevant molecules, particularly given the importance that heterocycles have in biological environments.

Author contributions

D. G.: investigation, methodology, writing – original draft. G. C.: investigation; P. N. Z.: formal analysis, visualization; P. P. M.: validation; A. B.: writing – review & editing; L. C.: visualization; D. M. P.: formal analysis, visualization; P. P.: conceptualization, writing – review editing.

Conflicts of interest

There are no conflicts to declare.

Data availability

The data supporting this article have been included as part of the SI: optical and SEM images, NMR and IR spectra, TGA and PXRD traces, structural information. See DOI: **https://doi.org/10.1039/d5dt01321f**.

CCDC 2450669–2450672 contain the supplementary crystallographic data for this paper.[43a–d]

Acknowledgements

Chiesi Farmaceutici S.p.A. is acknowledged for the use of the Bruker D8 Venture single-crystal diffractometer. The Laboratorio di Strutturistica “M. Nardelli” of the University of Parma is acknowledged for the X-ray diffraction data collection. The Centro Interdipartimentale di Misure (CIM) of the University of Parma is thanked for instrument facilities. Dr Ferdinando Vescovi (University of Parma) is thanked for the acquisition of SEM images. We thank Prof. Vladislav A. Blatov at the Samara Center for Theoretical Materials Science for providing free ToposPro software (**https://topospro.com**).

References

1 M. D. Allendorf, M. E. Foster, F. Léonard, V. Stavila, P. L. Feng, F. P. Doty, K. Leong, E. Y. Ma, S. R. Johnston and A. A. Talin, *J. Phys. Chem. Lett.*, 2015, **6**, 1182–1195.
2 H. Vardhan, M. Yusubov and F. Verpoort, *Coord. Chem. Rev.*, 2016, **306**, 171–194.

3 Y. Inokuma, S. Yoshioka, J. Ariyoshi, T. Arai, Y. Hitora, K. Takada, S. Matsunaga, K. Rissanen and M. Fujita, *Nature*, 2013, **495**, 461–466.
4 A. D. Cardenal and T. R. Ramadhar, *ACS Cent. Sci.*, 2021, **7**, 406–414.
5 Q. Du, J. Peng, P. Wu and H. He, *TrAC, Trends Anal. Chem.*, 2018, **102**, 290–310.
6 N. Zigon, V. Duplan, N. Wada and M. Fujita, *Angew. Chem., Int. Ed.*, 2021, **60**, 25204–25222.
7 D. Balestri, P. P. Mazzeo, C. Carraro, N. Demitri, P. Pelagatti and A. Bacchi, *Angew. Chem., Int. Ed.*, 2019, **58**, 17342–17350.
8 P. P. Mazzeo, D. Balestri, A. Bacchi and P. Pelagatti, *CrystEngComm*, 2021, **23**, 7262–7269.
9 D. Balestri, P. P. Mazzeo, R. Perrone, F. Fornari, F. Bianchi, M. Careri, A. Bacchi and P. Pelagatti, *Angew. Chem., Int. Ed.*, 2021, 10194–10202.
10 Y. Zhang, L. Chang, N. Yan, Y. Tang, R. Liu and B. E. Rittmann, *Environ. Sci. Technol.*, 2014, **48**, 649–655.
11 Y. Bai, Q. Sun, R. Xing, D. Wen and X. Tang, *J. Hazard. Mater.*, 2010, **181**, 916–922.
12 W. Kang, Y. Cui, Y. Yang, M. Guo, Z. Zhao, X. Wang and X. Liu, *J. Hazard. Mater.*, 2021, **417**, 126160.
13 B. Tan, Z. F. Wu, M. Z. Jia, J. Zhang and G. Y. Yang, *Inorg. Chem.*, 2023, **62**, 6688–6695.
14 P. W. Seo, I. Ahmed and S. H. Jhung, *Chem. Eng. J.*, 2016, **299**, 236–243.
15 I. Ahmed, N. A. Khan, Z. Hasan, S. H. Jhung and J. Hazard, *Materials*, 2013, **250–251**, 37–44.
16 D. Balestri, D. Capucci, N. Demitri, A. Bacchi and P. Pelagatti, *Materials*, 2017, **10**, 727.
17 F. Sakurai, A. Khutia, T. Kikuchi and M. Fujita, *Chem. – Eur. J.*, 2017, **23**, 15035–15040.
18 F. Habib, D. A. Tocher and C. J. Carmalt, *CrystEngComm*, 2023, **25**, 5001–5011.
19 Z. Hasan, M. Tong, B. K. Jung, I. Ahmed, C. Zhong and S. H. Jhung, *J. Phys. Chem. C*, 2014, **118**, 21049–21056.
20 M. J. Kim, S. M. Park, S. J. Song, J. Won, J. Y. Lee, M. Yoon, K. Kim and G. Seo, *J. Colloid Interface Sci.*, 2011, **361**, 612–617.
21 G. C. Laredo, P. M. Vega-Merino, J. Ascención Montoya-De La Fuente, R. J. Mora-Vallejo, E. Meneses-Ruiz, J. Jesús Castillo and B. Zapata-Rendón, *Fuel*, 2016, **180**, 284–291.
22 D. Balestri, I. Bassanetti, S. Canossa, C. Gazzurelli, A. Bacchi, S. Bracco, A. Comotti and P. Pelagatti, *Cryst. Growth Des.*, 2018, **18**, 6824–6832.
23 A. Delledonne, M. Orlandini, F. Terenziani, P. P. Mazzeo, A. Bacchi, L. Carlucci, A. Comotti, J. Perego and P. Pelagatti, *CrystEngComm*, 2023, **25**, 2085–2095.
24 F. Bianchi, A. Pankajakshan, F. Fornari, S. Mandal, P. Pelagatti, A. Bacchi, P. P. Mazzeo and M. Careri, *Microchem. J.*, 2020, **154**, 1–7.
25 P. Giovanardi, D. Ribezzi, E. Napolitano, M. Orlandini, M. Riboni, N. Mazzeo, P. P. Bacchi, A. Bianchi, F. Careri and M. Pelagatti, *Chem. – Eur. J.*, 2025, **31**, e202501167.
26 D. Giovanardi, P. P. Mazzeo, P. Pelagatti and A. Bacchi, *Cryst. Growth Des.*, 2023, **23**, 8726–8734.
27 G. M. Sheldrick, *Acta Crystallogr., Sect. A:Found. Adv.*, 2015, **71**, 3–8.
28 G. M. Sheldrick, *Acta Crystallogr., Sect. C: Struct. Chem.*, 2008, **64**, 112.
29 O. V. Dolomanov, L. J. Bourhis, R. J. Gildea, J. A. K. Howard and H. Puschmann, *J. Appl. Crystallogr.*, 2009, **42**, 339–341.
30 A. L. Spek, *Acta Crystallogr., Sect. C: Struct. Chem.*, 2015, **71**, 9–18.
31 G. B. P. Ugliengo and D. Viterbo, *J. Appl. Crystallogr.*, 1988, **21**, 75.
32 P. M. Chuang, P. R. Li and J. Y. Wu, *Dalton Trans.*, 2024, **2**, 1884–1895.
33 R. Kumar, A. Thakur Sachin, D. Chandra, A. Kumar Dhiman, P. Kumar Verma and U. Sharma, *Coord. Chem. Rev.*, 2024, 499.
34 L. L. Merritt, R. T. Cady and B. W. Mundy, *Acta Crystallogr.*, 1954, **7**, 473–476.
35 G. J. Palenik, *Acta Crystallogr.*, 1964, **17**, 687.
36 Z. F. Chen, M. Zhang, S. M. Shi, L. Huang, H. Liang and Z. Y. Zhou, *Acta Crystallogr., Sect. E:Struct. Rep. Online*, 2003, **59**, 814–815.
37 G. Varelas, A. Salifoglou and V. Psycharis, *Acta Crystallogr., Sect. C:Cryst. Struct. Commun.*, 2013, **69**, 868–871.
38 D. Balestri, A. Bacchi, P. Scilabra and P. Pelagatti, *Inorg. Chim. Acta*, 2017, **470**, 416–122.
39 V. A. Blatov, A. P. Shevchenko and D. M. Proserpio, *Cryst. Growth Des.*, 2014, **14**, 3576–3586.
40 K. Chang, C. Huang, Y. Liu, Y. Hu, P. Chou and Y. Lin, *Dalton Trans.*, 2004, 1731–1738.
41 M. Lõkov, S. Tshepelevitsh, A. Heering, P. G. Plieger, R. Vianello and I. Leito, *Eur. J. Org. Chem.*, 2017, **2017**, 4475–4489.
42 R. S. Hosmane and J. F. Liebman, *Struct. Chem.*, 2009, **20**, 693–697.
43 (*a*) P. P. Mazzeo, CCDC 2450669 (**PUM168@(quino)$_1$**): Experimental Crystal Structure Determination, 2025, DOI: **10.5517/ccdc.csd.cc2n83vx**; (*b*) P. P. Mazzeo, CCDC 2450670 (**PUM168@(quino)$_7$**): Experimental Crystal Structure Determination, 2025, DOI: **10.5517/ccdc.csd.cc2n83wy**; (*c*) P. P. Mazzeo, CCDC 2450671 (**PUM210@(quino)$_1$**): Experimental Crystal Structure Determination, 2025, DOI: **10.5517/ccdc.csd.cc2n83xz**; (*d*) P. P. Mazzeo, CCDC 2450672 (**PUM210_PY**): Experimental Crystal Structure Determination, 2025, DOI: **10.5517/ccdc.csd.cc2n83y0**.